Transmittance of a tuneable filter at terahertz frequencies

Timothy D. Drysdale

Department of Electronics and Electrical Engineering,

University of Glasgow, Glasgow, G12 8LT, United Kingdom

Ian S. Gregory, Colin Baker

Semiconductor Physics Group, Cavendish Laboratory,

University of Cambridge, Madingley Road, Cambridge,

CB3 0HE, United Kingdom and Teraview Ltd,

Unit 302/304 Cambridge Science Park, Milton Road,

Cambridge, CB4 0WG, United Kingdom

Edmund H. Linfield

Semiconductor Physics Group, Cavendish Laboratory,

University of Cambridge, Madingley Road, Cambridge, CB3 0HE

William R. Tribe

Teraview Ltd, Unit 302/304 Cambridge Science Park,

Milton Road, Cambridge, CB4 0WG, United Kingdom

David R. S. Cumming*

Department of Electronics and Electrical Engineering,

University of Glasgow, Glasgow, G12 8LT, United Kingdom

Abstract

A metallic photonic crystal filter has been demonstrated at terahertz frequencies, with the pass-band tuneable over the range 365 - 386 GHz. Tuning is achieved by a relative lateral shift of two metallic photonic crystal plates. Each plate comprises two orthogonal layers of gratings and integral mounting lugs. The plates are micromachined from silicon wafers then coated in gold to provide metallic electromagnetic behaviour. An insertion loss of 3 – 7 dB and Q in the range 20 – 30 was achieved. A shift of 140 μm gave a tuning range of 21 GHz, tuning sensitivity of 150 GHz/mm and a fractional tuning range of 6%.

Terahertz frequency imaging systems are attracting a growing interest as they improve in both speed and cost[1]. These developments lead the way for a diverse range of emerging applications in spectroscopy and imaging that require additional passive components, such as tuneable filters. For example, tuneable filters are an inline and compact replacement for diffraction gratings and moveable slits in spectrometers employing bolometric detection and facilitate inexpensive frequency agility in broadband pico-cellular or intra-satellite communications networks. In other applications, benefits accrue from installing a filter that is continuously tuneable, such as providing tuneable operating frequencies and improved tolerance to manufacturing variations.

A number of high frequency filters have been reported to date. These include fixed frequency filters operating in the range 100 GHz - 20 THz[2–4] or devices that are on-off switchable from fixed pass-band to all-reject[5]. Continuously tuneable filters have previously only been demonstrated for operation up to 30 GHz[6] or 100 GHz[7]. In this letter, we report the fabrication and characterization of a filter that is continuously tuneable by means of a mechanical motion, based on a metallic photonic crystal at terahertz frequencies. The filter is designed for free-space operation and is constructed from two identical plates, as shown in Fig. 1 (not to scale, and with a cut-away for clarity)[8,9]. Each plate comprises two orthogonal linear grids with integral mounting lugs. Linearly polarized waves, having the electric field **E** orientation as shown (transverse magnetic, TM), are normally incident from the top of the device. The TM polarization direction is chosen in order to access the tuning mode we describe here. For the orthogonal polarization (transverse electric), there is no tuning mechanism within or below the frequency range of interest, since transmission is blocked due to an effect similar to a simple wiregrid polarizer. Therefore we confine the remainder of our discussion to the TM polarization. All the rods in the grids are of subwavelength size, having dimensions of

width r, depth d, and period Λ.

The transmission characteristic of this filter exhibits a plasmonic forbidden band that extends from zero frequency to a cutoff frequency f_c where the wavelength is approximately equal to twice the lattice constant of the three dimensional lattice structure[10] ($\lambda_0 \approx 2\Lambda$). There is a single peaked transmission band located just above f_c, which may be continuously tuned by a relative lateral shift, $0 < s < \Lambda_2$, of the plates in a direction parallel to the inner grids' grating vector $\mathbf{K}$. An allowance is made for a small fixed separation g between the plates but this is not used to tune the device, therefore the tuning method is different to Fabry-Pérot cavity-based techniques[6,11]. Ideally $g = 0$, but practical designs to facilitate translation of the plates require a small degree of separation. In the initial position, the inner rods are aligned ($s = 0$, not shown in Fig. 1) and the passband frequency f_p is at its highest. Increasing the tuning shift s causes f_p to fall.

We developed a wavelength scaleable micro-fabrication process[9] based on a double-sided inductively-coupled plasma deep reactive ion etch (DRIE) of a silicon wafer. The design dimensions of the 375 GHZ filter were $r = 110\,\mu$m, $d = 115\,\mu$m, and $\Lambda = 440\,\mu$m. The central gridded area was 20 mm $\times$ 20 mm while the over-all plate size (i.e. including the mounting lugs with their 3 mm holes) was 22 mm $\times$ 38 mm. Due to slight variations in the DRIE conditions between fabrication runs, scanning electron micrographs of the plates indicated that the rod widths r were $97\,\mu$m and $109\,\mu$m in the middle of the upper and lower layers of the first plate respectively, and $87\,\mu$m and $107\,\mu$m for the second plate. After etching, the silicon plates were coated in gold using a three step metallization process. First, 40 nm of Ti was electron beam evaporated onto both sides of the device to improve adhesion. Next, 40 nm of Au was sputtered onto all surfaces. Finally, electroplating was used to increase the thickness to approximately $1.2\,\mu$m, so that incident electric fields at

the frequencies of interest cannot penetrate through to the dielectric core. Thus the device behaves electromagnetically as if it is constructed from solid gold.

Terahertz measurements were conducted in the frequency range 50 – 800 GHz, using a broadband pulsed THz system[1]. A femtosecond laser produced 120 fs pulses with a central wavelength of 1.06 μm at a repetition rate of 75 MHz. The laser output was split into pump and probe components using a beam splitter. The pump component was focused onto the feedpoint of an antenna fabricated on a low temperature (LT) InGaAs photoconductive emitter, and the bias applied to the antenna was modulated at 25 kHz to facilitate lock-in detection. The photoconductive switching causes current transients within the semiconductor, which in turn produces a broadband pulse of terahertz radiation. A 25 mm diameter (22 mm aperture) silicon hyperhemispherical lens couples radiation out of the rear surface of the emitter, producing a collimated beam in free space. An off-axis $f_1 = 50$ mm aluminium parabolic mirror focuses the beam to a diameter of $\simeq 6$ mm, onto the filter device, as shown in Fig. 2. An off-axis $f_2 = 100$ mm gold-plated parabolic mirror collects the transmitted terahertz radiation, and recollimates it for detection onto an unbiased photoconductive detector that is similar in design to the device used at the source. The amplitude of the THz pulse is detected via the induced current flow, measured by optically gating the detector with pulses from probe component of the laser output. An 96 mm long variable delay line is incorporated into the receiver optics so that the time delay between the incoming THz pulse and the probe pulse can be varied over 640 ps in steps of 0.3 ps. This allows Fourier decomposition of the broadband frequency spectrum, with 1.5 GHz frequency resolution.

Transmission through the device was measured in twelve different tuning positions, at steps of 20 μm in the range $0 < s < 220\,\mu$m. Actuation was provided by differential micrometers and a three axis translation stage, upon which one plate was mounted over both a Tufnel

and an absorbing foam aperture of 20 mm×20 mm. The second plate was mounted on an identical fixed aperture. For this experiment, the plates were attached to the Tufnel holders with silver dag and aligned by eye with the aid of a microscope. A reference measurement was taken of the entire setup without the filter plates in place for calibration purposes.

The measurement results are plotted in Fig. 3, with the transmission for two representative tuning positions ($s = 0, 140\,\mu$m) shown in the main graph and a plot of the centre frequency f_p and the -3 dB points of the main tuning peak, plotted as a function of s for all twelve measured tuning positions, is shown in the inset. At $s = 0\,\mu$m, $f_p = 386$ GHz and falls to its lowest value of $f_p = 365$ GHz at $s = 140\,\mu$m, giving a tuning sensitivity of 21 GHz/140 μm or 150 GHz/mm. The insertion loss and Q at $s = 0\,\mu$m is 3.7 dB and 20 respectively, rising in both cases to 7.1 dB and 30 at $s = 140\,\mu$m. Once the maximum tuning shift is reached at $s = 140\,\mu$m, the centre frequency does not rise again as strongly as reported previously for a lower frequency device[8]. We believe that this is due to the measured gap between the plates of 30 μm in both experiments having a greater effect at the shorter wavelengths studied in this work. Over the range $0 < s < 140\,\mu$m, the Δf_p-FWHM ratio is 1.6 relative to the peak with the highest Q ($s = 140\,\mu$m), and 1.1 relative to the peak with the lowest Q ($s = 0\,\mu$m). The fractional tuning range is $2\Delta f_p/(f_{p_{min}} + f_{p_{max}}) = 6\,\%$.

The performance of the device was predicted using full-vector electromagnetic finite-difference time-domain (FDTD) simulations. In order to achieve practical simulation times, it was necessary to model the device as an infinite grid by surrounding a unit cell of the device with periodic boundary conditions, due to the computationally intensive nature of FDTD. We believe this approach is justified because we do not observe edge effects in the measured results unless the optics are deliberately misaligned. The complete frequency response over the range of frequencies of interest was obtained in a single simulation by

exciting the structure with a normally-incident plane wave with a Gaussian envelope and taking a fast Fourier transform of the transmitted fields. The cell size was 5 μm and the simulation domain was 88 × 88 × 396 cells. Simulations were performed for the measured gap of 30 μm using the same values for s as shown in the experimental data of Fig. 3. The structures were represented by perfect electrical conductors; this approach is consistent with other studies at these frequencies[12,13] that neglect absorption of metals below 1 THz.

The simulation results are plotted in Fig. 4, with the transmission characteristics shown in the main graph and a plot of the centre frequency f_p and the -3 dB points of the main tuning peak, plotted as a function of the same s values as in the experimental data, shown in the inset. At $s = 0\,\mu$m, $f_p = 363$ GHz and falls to its lowest value of $f_p = 342$ GHz at $s = 140\,\mu$m, giving a tuning sensitivity of 21 GHz/140 μm or 150 GHz/mm. The insertion loss and Q at $s = 0\,\mu$m is 0.4 dB and 16 respectively, rising in both cases to 0.6 dB and 19 at $s = 140\,\mu$m. Once the maximum tuning shift is reached at $s = 140\,\mu$m, the centre frequency rises only slightly, by 1 GHz when s is increased to $s = 220\,\mu$m. Over the range $0 < s < 140\,\mu$m, the Δf_p-FWHM ratio is 1.1 relative to the peak with the highest Q ($s = 140\,\mu$m), and 0.9 relative to the peak with the lowest Q ($s = 0\,\mu$m). Other simulations, not shown here, indicate that for $g = 0\,\mu$m, the tuning range increases to 78 GHz(309 GHz< f_p <387 GHz) for a tuning sensitivity of 557 GHz/mm, an improved Δf_p-FWHM ratio of 4 and a fractional tuning range of 22 %. This indicates that the measured performance of the filter could therefore be improved by reducing g, from its present value of 30 μm, using more advanced plate alignment techniques. It is noted that the same tuning range and behaviour is predicted and measured, except for a slight offset in the absolute frequency (approximately 23 GHz or 6%) which we partially attribute to the error in quantizing the structure's geometry into the 5 μm grid of the simulation domain and non-uniform rod dimensions in the actual device.

Key performance parameters of our tuneable filter, such as peak transmission (-3.7 dB) and Q (20), compare favourably with other terahertz filters, despite the added technical difficulties of creating a continuously tuneable device. The on-off tuneable filter[5] did have better Q (76) but at the expense of reduced peak transmission (-27 dB).

In conclusion, we have demonstrated a filter with a continuously tuneable passband at terahertz frequencies. The filter relies on the tuning of a metallic photonic crystal through a relative lateral shift of two silicon-microfabricated plates that have been coated in thick gold. The device was characterized in a broad-band terahertz pulsed imaging system. Full vector electromagnetic FDTD simulations were used to predict the device performance. The filter's measured insertion loss was higher than expected at between 3 – 7 dB, although this is expected to be acceptable for application at terahertz frequencies. A tuning range of 21 GHz (365 GHz $< f_p <$ 386 GHz) and passband a Q of between 20 to 30 was achieved in good agreement with simulations.

This work was supported by Scottish Enterprise's Proof of Concept Fund. EHL acknowledges the support of Toshiba Research Europe Ltd.

* Author to whom all correspondence should be addressed; electronic mail: d.cumming@elec.gla.ac.uk

[1] C. Baker, I. S. Gregory, W. R. Tribe, I. V. Bradley, M. J. Evans, M. Withers, P. F. Taraday, V. P. Wallace, E. H. Linfield, A. G. Davies, and M. Missous. *Appl. Phys. Lett.* **83**, 4113 (2003).

[2] H. A. Smith, M. Rebbert and O. Sternberg, *Appl. Phys. Lett.* **82**, 3605 (2003).

[3] D. Wu, N. Fang, C. Sun, X. Zhang, W. J. Padilla, D. N. Basov, D. R. Smith and S. Schultz, *Appl. Phys. Lett.* **83**, 201 (2003).

[4] D. W. Porterfield, J. L. Hesler, R. Densing, E. R. Mueller, T. W. Crowe, and R. M. Weikle II. *Appl. Opt.* **33**, 6046 (1994).

[5] J.-M. Lourtioz, A. de Lustrac, F. Gadot, A. Chelnokov, T. Brillat, A. Ammouche, J. Danglot, O. Vanbésien, and D. Lippens. *J. Lightwave Tech.* **17**, 2025 (1999).

[6] B. Temelkuran, H. Altug, and E. Ozbay. *IEE Proc. Optoelectronics* **145**, 409 (1998).

[7] J. P. Gianvittorio, J. Zendejas, Y. Rahmat-Samii, and J. Judy. *Electron. Lett.* **38**, 1627 (2002).

[8] T. D. Drysdale, R. J. Blaikie, and D. R. S. Cumming. *Appl. Phys. Lett.* **83**, 5362 (2003).

[9] T. D. Drysdale, G. Mills, S. M. Ferguson, R. J. Blaikie, and D. R. S. Cumming. *J. Vac. Sci. Technol. B* **21**, 2878 (2003).

[10] D.F. Sievenpiper, M.E. Sickmiller, and E. Yablonovitch, Phys. Rev. Lett. **76**, 2480 (1996).

[11] R. Ulrich, T. J. Bridges, and M. A. Pollack. Variable metal mesh coupler for far infrared lasers. *Appl. Opt.* **9**, 2511 (1970).

[12] S. Fan, P.R. Villeneuve, and J. D. Joannopoulos, Phys. Rev. B **54**, 11245 (1996).

[13] M. M. Sigalas, C. T Chan, K. M. Ho, and C. M. Soukoulis. *Phys. Rev. B* **52**, 11744 (1995).

List of Figure Captions

Fig. 1. Diagram of the filter's construction, comprising two identical gold-coated micro-fabricated silicon plates (shown not to scale and cut-away for clarity). The rod dimensions are width r, depth d and period Λ. Tuning is achieved by a relative lateral shift of the plates s in a direction parallel to the inner grids' grating vector $\mathbf{K}$.

Fig. 2. Schematic layout of the terahertz measurement setup. A femtosecond laser (not shown) with $\lambda = 1.06\,\mu$m provides 120 fs pulses to both the emitter and detector (fabricated on LT InGaAs). Silicon lenses couple radiation to/from the antennae while the filter is placed at the focus of two parabolic mirrors.

Fig. 3. Plot of the measured transmission coefficient of the filter for two tuning positions ($s = 0, 140\,\mu$m.) The inset shows the tuning of the passband peak and -3dB points for all twelve measured tuning positions.

Fig. 4. Plot of the simulated transmission coefficient of the filter for the same two tuning positions ($s = 0, 140\,\mu$m) as in Fig. 3. The inset shows the tuning of the passband peak and -3dB points for all twelve simulated tuning positions.

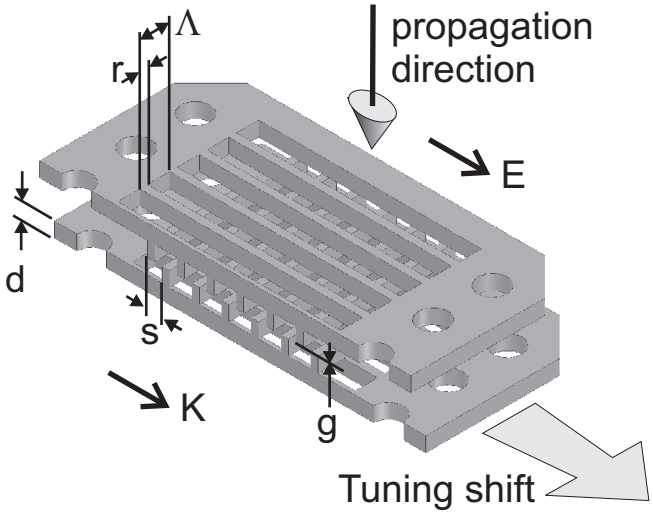

FIG. 1: Drysdale et. al., *Applied Physics Letters*

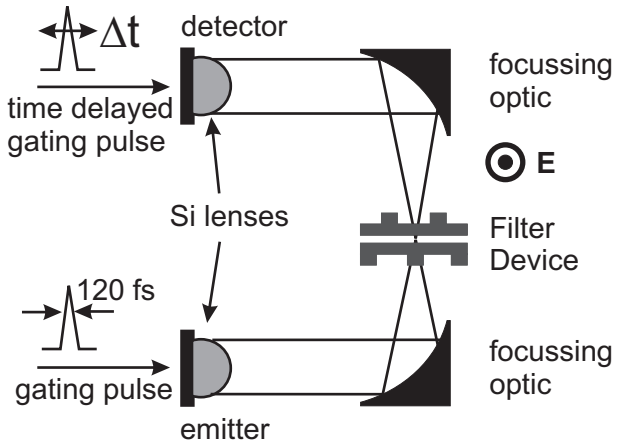

FIG. 2: Drysdale et. al., *Applied Physics Letters*

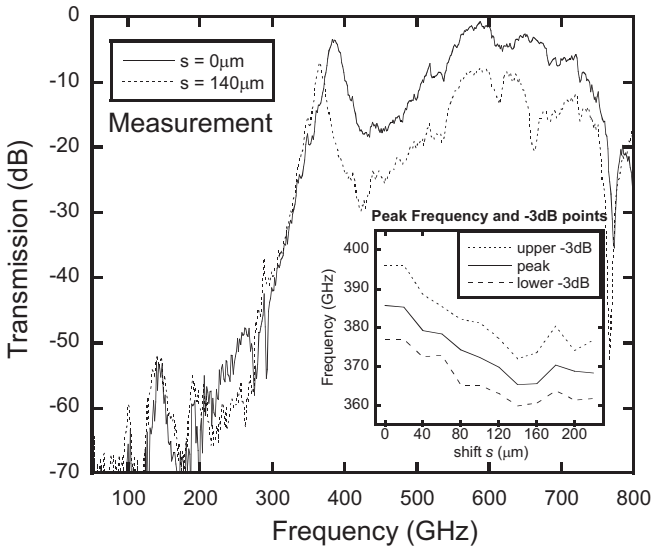

FIG. 3: Drysdale et. al., *Applied Physics Letters*

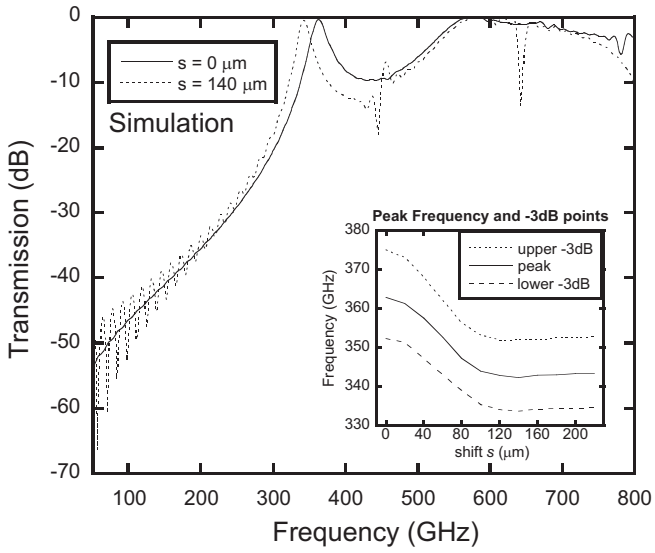

FIG. 4: Drysdale et. al., *Applied Physics Letters*